Accepted Manuscript

Title: Indiscriminate Revelation of Dislocations in Single Crystal SiC by Inductively Coupled Plasma Etching

Authors: Yi Zhang, Rulin Li, Yongjie Zhang, Dianzi Liu, Hui Deng

PII: S0955-2219(19)30185-2
DOI: https://doi.org/10.1016/j.jeurceramsoc.2019.03.026
Reference: JECS 12400

To appear in: *Journal of the European Ceramic Society*

Received date: 25 January 2019
Revised date: 7 March 2019
Accepted date: 10 March 2019

Please cite this article as: Zhang Y, Li R, Zhang Y, Liu D, Deng H, Indiscriminate Revelation of Dislocations in Single Crystal SiC by Inductively Coupled Plasma Etching, *Journal of the European Ceramic Society* (2019), https://doi.org/10.1016/j.jeurceramsoc.2019.03.026

This is a PDF file of an unedited manuscript that has been accepted for publication. As a service to our customers we are providing this early version of the manuscript. The manuscript will undergo copyediting, typesetting, and review of the resulting proof before it is published in its final form. Please note that during the production process errors may be discovered which could affect the content, and all legal disclaimers that apply to the journal pertain.

ACCEPTED MANUSCRIPT

# Indiscriminate Revelation of Dislocations in Single Crystal SiC by Inductively Coupled Plasma Etching

*Yi Zhang[1,2], Rulin Li[1], Yongjie Zhang[1], Dianzi Liu[2] and Hui Deng[1, *]*

1. Department of Mechanical and Energy Engineering, Southern University of Science and Technology, No. 1088, Xueyuan Road, Shenzhen, Guangdong 518055, China
2. Engineering, Faculty of Science, University of East Anglia, Norwich Research Park, Norwich, NR4 7TJ, UK

ACCEPTED MANUSCRIPT

**Abstract**

To reveal dislocations in SiC wafers, conventionally, molten KOH etching method has been widely used. However, when highly doped sites exist on the wafer, the molten KOH etching method is not applicable owing to the enhanced isotropic electrochemical etching phenomenon. In this study, plasma etching is first applied to reveal dislocations in a 4H-SiC wafer with both highly doped and lightly doped areas. The mechanisms of dislocation revelation by dry etching have been theoretically analyzed and it has been revealed that the dislocation revelation ability of dry etching is highly related to the temperature of the etching process. The results demonstrate that inductively coupled plasma (ICP) etching can maintain its effectiveness for dislocation revelation of SiC wafers regardless of the

ACCEPTED MANUSCRIPT

doping concentrations. This work offers an alternative approach to indiscriminately and accurately reveal dislocations in SiC wafers.

Keywords:

single crystal SiC; etching; dislocation; inductively coupled plasma; etch pit

ACCEPTED MANUSCRIPT

ACCEPTED MANUSCRIPT

## 1. Introduction

Single crystal silicon carbide (4H-SiC) has many excellent electrical, mechanical and chemical properties such as wide bandgap, high thermal conductivity, strong chemical inertness and high hardness, making it one of the most promising semiconductor materials for next-generation electronic devices working in high voltage, high frequency and high temperature conditions.[1-2] For the manufacturing of SiC-based electronic device, 4H-SiC wafers with low defect density and good surface quality are indispensable. With decades of efforts by numerous researches, the quantity of micropipes defects has been reduced greatly.[3-4] However, the density of elementary dislocations like threading screw dislocations (TSDs), threading edge dislocations (TEDs) and basal plane dislocations (BPDs) is still remains very high (~$10^4$ $cm^{-2}$), which significantly degenerates the electrical performance of SiC devices.[5-6] As the dislocation density is a key parameter of a SiC wafer, a convenient, time efficiency and broad-spectrum dislocation detection method is highly needed.

Molten KOH etching is the conventional method to detect the dislocations in a 4H-SiC wafer.[7] During the etching process, defects will be preferentially attacked due to energy relaxation, and thus can be identified as etching pits.[8] As reported, this method is highly efficient to reveal dislocation for SiC with p-type doping or moderate n-type doping ($n<10^{18}cm^{-3}$).[9-10] After the Si-face (0001) of 4H-SiC was etched by molten KOH, TSDs and TEDs will be revealed as hexagonal etching pits with relatively large and small size respectively, and BPDs as seashell-shape etching pits.[11] However, the failure of conventional molten KOH etching method have been widely reported when conducted on highly doped n-type SiC wafers ($n > 10^{18}cm^{-3}$). The reveled etching pits density (EPD) will

ACCEPTED MANUSCRIPT

be much lower than the real defect density, and the shape of etching pits will turn to be oval and undistinguishable.[10, 12-13] Gao et al.[12] suggested that the etching effect of molten KOH method for SiC contains both chemical and electrochemical reaction, during which isotropic etching and preferential etching are competitive. For p-type and low doping n-type SiC wafers, electrochemical reaction is limited due to the lack of carriers in the depletion layer on the solid-liquid interface. Preferential chemical reaction happens and defects are selectively etched. However, for high doping n-type SiC wafers, isotropic electrochemical reaction is enhanced by the inversion layer on the solid-liquid interface. In such case, the defect sites and non-defect sites are homogeneously etched and KOH etching lost its effectiveness of defect detection. Huge different of electrochemical etching rate of SiC for different doping concentration during anodizing oxidation has also been reported.[14] Therefore, it is a great challenge to detect the dislocation density of highly doped SiC wafers.

To conduct defect selective etching on a highly doped n-type SiC wafer, isotropic electrochemical reaction must be limited meanwhile the preferential chemical etching of dislocation sites must be enhanced. One solution is to find an etching process in which the formation of the inversion layer on the solid-liquid interface can be limited and isotropic electrochemical etching can be eliminated. Plasma etching, which is a dry etching process, meets this requirement well. In addition, plasma etching can be highly selective to defects due to the higher material removing rate at dislocation sites caused by the lower stability of dislocation structures compared to perfect crystal lattices.[15]

In this study, we proposed a plasma dry etching process for dislocation revelation of 4H-SiC regardless of the doping concentration. Two different type of plasma source have

ACCEPTED MANUSCRIPT

been built to investigate the etching mechanisms. It has been theoretically and experimentally revealed that the dislocation revelation ability is highly related to the temperature of the etching process. We proved that ICP etching can be very efficient in doping-density-independent dislocation revelation of 4H-SiC.

## 2. Experimental section

Material: Commercially available n-type 4H-SiC wafer (on-axis), with a thickness of 365 μm and doping concentration of $10^{18}$-$10^{19}$cm$^{-3}$ were used in this research. All experiments were conducted on the Si (0001) face, which is also the most commonly used face for power device applications.

Molten KOH etching: For the conventional molten KOH etching method, the SiC sample is placed in a nickel crucible full with KOH. This crucible is then put into a muffle furnace and heat to 510 °C within 50 mins, and hold in this temperature for 4 mins, then cooling to room temperature within 60 mins. After the cooling process, the etched sample is washed in deionized (DI) water with ultrasonic cleaning machine to remove all the KOH.

CCP etching: For the CCP etching method, the equipment we use is shown in Figure 2b. A RF power (13.56 MHz, 50 W) is connected to two concentric electrodes which separated by a dielectric tube (Alumina) and a PTFE chamber. PTFE material is only used in place where there is no direct contact with fluorine radical to avoid the etching loss. For position where high density of fluorine radical generates, alumina dielectric tube is used to prevent the arc discharge and etching. The central electrode is made of aluminum alloy as it will form a passivation layer after being oxidized which can prevent

ACCEPTED MANUSCRIPT

corrosion of fluorine radical and the ground electrode of stainless steel. A gas mixture (He: 5 slm, $CF_4$: 20 sccm, $O_2$: 10 sccm) is introduced into the chamber tangentially. When this mixed gas flows through the annular gap between the two electrodes where RF power is applied, glow discharge is ignited in this gap and a plasma plume reaching length up to 1 cm is launched though the nozzle to the ambient air. The temperature of this plasma is around 50 °C due to the small applied power of the non-equilibrium gas discharge. This plasma is then used to etching SiC in a scan path with a 2 mm distance between the plasma nozzle and sample and the scan time is 20 mins.

ICP etching: the ICP plasma setup is shown in Figure 4b. A quartz torch is connected to a three-channel gas supporting system. The quartz torch contains three concentric tubes, the outer tube is supplied with cooling gas, which is pure argon with a flow rate of 13.0 slm. The second tube is supplied with pure argon with a flow rate of 1.5 slm as the plasma ignition gas. And the central tube is supplied with reactive gas, which is $CF_4$ and its flow rate is 30 sccm in the etching experiments. The bottom of the quartz torch is placed in the center of an inductance coil, which is connect to a RF power (40.68 MHz, 1000 W) through a matcher. This RF power will induce a strong magnetic field in the center of the quartz torch, which generates a dense plasma due to the circular region of the electric field that exists concentric to the coil. The SiC sample was placed on a wafer holder made of aluminum alloy. The scanning of the wafer holder was controlled by NC program to make the whole surface etched by the plasma and the scanning time is 5 mins. The etched sample was cleaned with DI water with ultrasonic vibration followed by characterization using SEM.

ACCEPTED MANUSCRIPT

Comparison test: To compare the doping-density-independent dislocation revelation ability of conventional molten KOH etching method and plasma etching method without the influence of different samples, one SiC sample with both high doping area and low doping area has been found (Figure 6a). The color of SiC wafer is highly related to its doping density. The high doping will change the electric properties of the sample, and thus change the optical absorption and performs deeper color in visual. This sample has been cut into 2 SiC sheets (approximately 10×20 $mm^2$ each), numbered sample 1 and sample 2. Both samples contain high doping area and low doping area. Sample 1 was etched by conventional molten KOH etching method and sample 2 by ICP etching method. All of them were then observed by SEM.

Characterization and measurement: 1. SEM (ZEISS merlin and HITACHI TM4000Plus) were employed to get the surface morphology of the samples. 2. To evaluate the temperature of the SiC samples during plasma etching, thermal camera (FLIR T660) was used. The emissivity of SiC sample was calibrated using the contact thermometer method: placing a SiC sample on a heat table, and increase the temperature to a high value. When the temperature stable, using a thermocouple and a thermal camera to measure the temperature of the same spot at the same time. On the basis of the different temperature measurement, the emissivity correction could be achieved. After that, the thermal camera is calibrated and can be used to measure the temperature of SiC samples accurately. 3. The composition of radicals in plasma was determined by an emission spectrometer (Ocean optics USB4000). 4. The morphological characteristics of the raw SiC surface and the CCP etched sample were evaluated using an AFM (BRUKER Dimension edge) with a tapping mode and a scanning frequency of 1.0 Hz. 5. To further

ACCEPTED MANUSCRIPT

ACCEPTED MANUSCRIPT

evaluate the dislocation revelation result, etching pits density (EPD) has been employed to show the density of dislocations exposed at the etched surface. The number of etching pits located in 4 observation sites (950 μm×1270 μm) were counted for each area to ensure statistic meaningfulness.

## 3. Results and discussion

### 3.1 Conventional Molten KOH Etching

4H-SiC samples with low doping concentration ($10^{18}$ $cm^{-3}$) and high doping concentration ($>10^{19}$ $cm^{-3}$) have been etched using this method, and the results are shown in Figure 1. After etching, the low doping area (Figure 1a) is covered with etching pits and three kinds of dislocations can be identified from the shape. TSDs and TEDs are reveled as hexagonal etching pits with relatively bigger and small size.[16] The etching pits caused by BPDs usually form seashell shape instead.[17] Some etching pits originated from TEDs have lost their hexagonal shape and turned to be oval. It means that even in the relatively low doping area, isotropic electrochemical etching is still significant.[12] This result also proves that conventional molten KOH etching method is very sensitive to the doping concentration of the SiC wafer. For the high doping area (Figure 1b), however, only few shallow etching pits could be found. And it is virtually impossible to recognize the dislocation type from the shape of the etching pits. On the basis of these results, it is concluded that using conventional molten KOH etching method to revelation dislocations for highly doped n-type 4H-SiC is impractical.

ACCEPTED MANUSCRIPT

ACCEPTED MANUSCRIPT

The mechanism of this phenomena has been discussed by Gao et al. in detail.[18] Molten KOH etching of SiC consists two parallel reactions: chemical reaction and electrochemical reaction, although there is no external bias. Chemical reaction will preferentially attack the defect spot due to energy relaxation of those places, thus it is selective to dislocations. While electrochemical etching in this case, is a kind of anode oxidation reaction and mainly depend on the availability of holes which shows no selectiveness to dislocations.[19] The competition between chemical reaction and electrochemical reaction defines the final morphology of the etched surface. Gao[18] suggest that When SiC is contacting with molten KOH, band bending will happen at the solid-liquid interface, analogous to the band bending in the SiC-HF interface observed by J. S. Shor et al.[20] For p-type SiC, the energy band bends downward (Figure 1c), forming a hole depletion layer. This layer contains no mobile holes and act like a barrier that prevent charge exchange therefore hinders electrochemical reaction. The dominate chemical reaction will preferentially attack the defect sites, thus dislocation revelation works well. In contrast, for sufficiently high doping n-type SiC (Figure 1d), the undue band bending will cause a p-type inversion layer at the interface, which provides substantial holes as free carrier.[21] Electrochemical reaction will then become dominate due to the abundant holes. Meanwhile, as the electrochemical reaction happens entirely depending on the availably of holes, the etching of the p-type inversion layer will be uniform regardless the present of defects. This leads to the failure of conventional KOH method when conduct dislocation revelation over high doping n-type SiC substrates.

ACCEPTED MANUSCRIPT

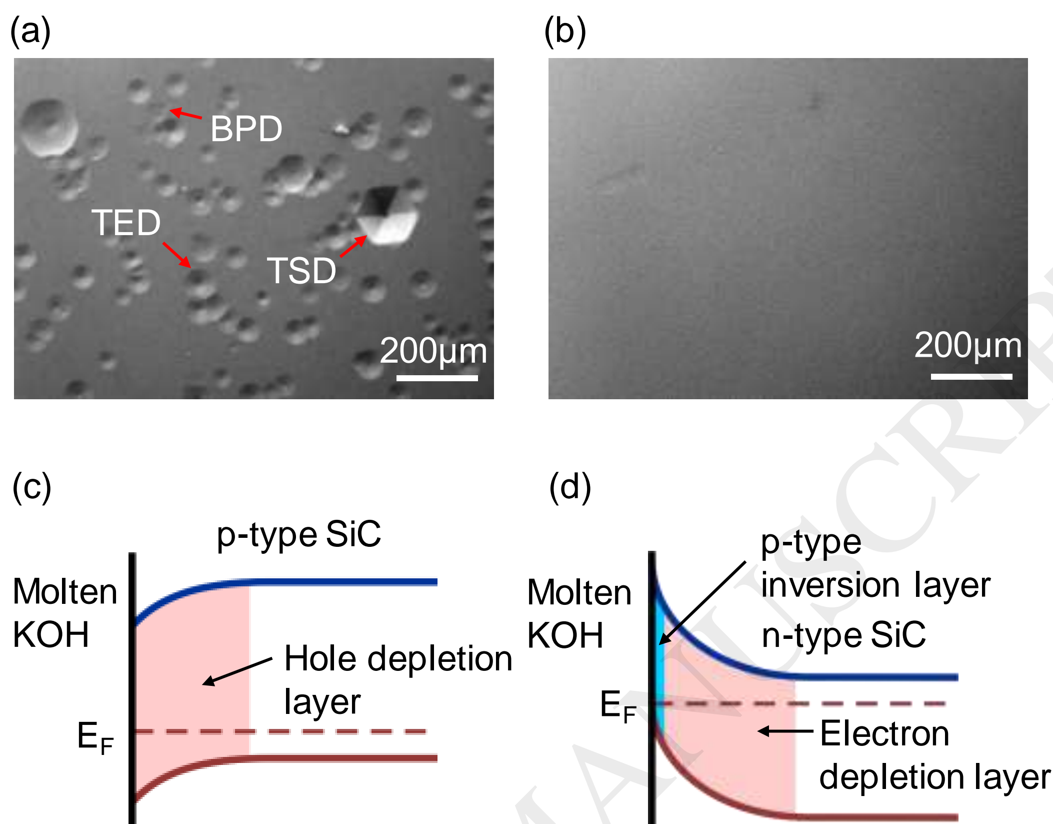


Figure 1. a, b) SEM images of the molten KOH etched surface of low doping SiC and high doping SiC. c, d) Band structure schematics of 4H-SiC/molten KOH interface for p-type SiC and high doping n-type

### 3.2 Capacitively coupled plasma (CCP) etching

To overcome the problem existing in conventional molten KOH etching method and find a new approach to realize doping-density-independent dislocation revelation, an etching process without electrochemical reaction must be find. One solution is choosing a kind of etching process without the solid-liquid interface, thus will prevent the band bending due to contact potential.[22] As a typical dry etching process, plasma etching does

ACCEPTED MANUSCRIPT

ACCEPTED MANUSCRIPT

not form the solid-liquid interface,[23] thus, electrochemical reactions, which invalidate the molten etching process, won't happen. Therefore, plasma dry etching is supposed to be effective to accurately reveal the dislocations in SiC wafers.

CCP is one of the most commonly used plasma source for semiconductor applications owing to its good stability and controllability.[24] With the capability to ignite discharge under atmospheric pressure, CCP can operate without the assist of expensive vacuum system.[25] Figure 2a shows the schematic of the CCP device used in this study and Figure 2b is the optical photo of the CCP jet. The chemical reactions occurring in the CCP etching process can be expressed as Equation (1):[26]

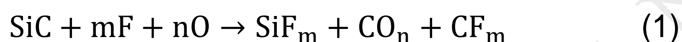

$$\mathrm{SiC + mF + nO \rightarrow SiF_m + CO_n + CF_m} \quad (1)$$

According to this equation, fluorine radicals and oxygen radicals are involved in the etching of SiC. Here, we choose $CF_4$ to be the fluorine source and $O_2$ as the oxygen source, and flow rates of them has been set to 20 sccm and 10 sccm respectively. To investigate the radicals inside the plasma, optical emission spectroscopy (OES) has been employed and the typical OES spectrum of the CCP jet at 50 W is shown in Figure 2c. Helium peaks (501, 587, 667, 706, 728 nm) which mainly formed due to the collision of energetic electrons with helium atoms can be seen clearly.[27-28] The oxygen atom emission at 777 nm and 844 nm are observable.[29] The nitrogen peaks (316, 337, 357, 380 nm), which comes from the participation of ambient air during plasma discharge, are also visible for the plasma jet.[28-29] The $CF_X$ continuum (ranges 280-400 nm) and $CF_3$ continuum (ranges 550-650 nm) are well pronounced.[30] Emissions from fluorine atoms

ACCEPTED MANUSCRIPT

(ranges 600-750 nm) are not very striking, due to their extremely short lives under atmospheric pressure.[31]

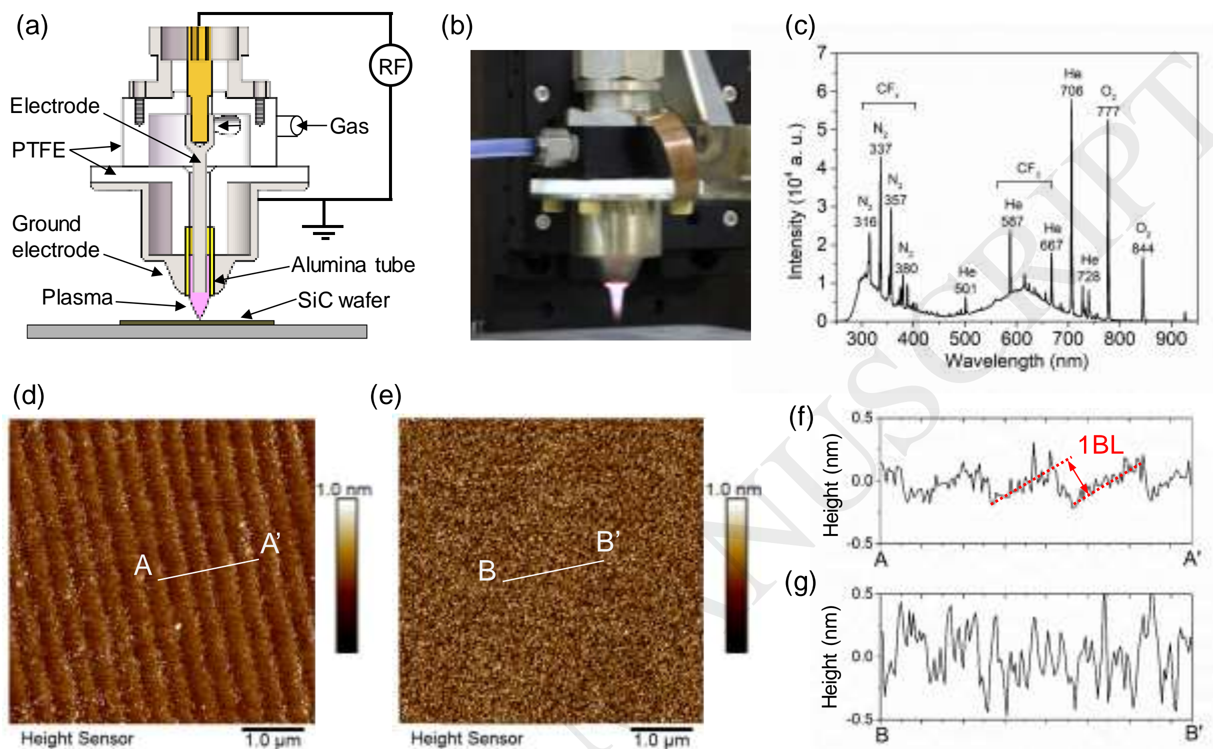


Figure 2. a) Schematic diagram of experimental setup for CCP jet etching. b) optical photo of the CCP jet. c) OES spectra of the CCP jet. d, e) AFM images of the Si face of 4H-SiC sample (d) before and (e) after CCP etching. f, g) Cross sectional profiles along A-A' and B-B' respectively.

This CCP jet was then employed to etch the Si-face of 4H-SiC. Figure 2d shows the raw surface before the treatment. Clear step-terrace structure suggests that the surface is well polished and not covered by other impurities. The step-terrace structure indicating the surface molecular fluctuation can also be seen in the surface cross sectional profile (Figure 2f). However, after etching, step-terrace structure disappeared and the surface

ACCEPTED MANUSCRIPT

became visually uniform covered with randomly distributed small pits or valleys (Figure 2e). From the cross-sectional profile (figure 2g) we can also observe that the etching was randomly occurred. The disappearing of step-terrace structure shows the etching was non-selectively to the step edges. The visually uniform surface implies it also has no preference to dislocation sites. These results suggest that roughly isotropic etching have been performed using CCP etching and it is not capable to revel dislocations.

ACCEPTED MANUSCRIPT

ACCEPTED MANUSCRIPT

### 3.3 Mechanism Speculation

To find out the reason why CCP etching only got a uniform surface without pronounced etching pits for dislocations, we measured the temperature of the sample during the CCP etching process. As shown in Figure 3a, the temperature of the SiC surface was lightly high than atmosphere temperature. The average substrate temperature was around 40 °C and maximum temperature was about 70 °C. The low temperature was considered as the reason for the results of isotropic etching shown in Figure 2e and the mechanism speculation has been given out as follows.

Figure 3b is the schematic of the cross section of a 4H-SiC sample with a threading dislocation line. The formation of etching pits is considered to be originated from the difference of etching rates between perfect crystalline surface and dislocation sites.[9] We assume the etching rate for perfect crystalline Si-face of 4H-SiC to be $v_p$, and the etching rate for the dislocation sites to be $v_d$. Etching rate $v_p$ is governed by Arrhenius equation:[32-33]

$$v_{\mathrm{p}} = n_{\mathrm{F}} A exp\left\{\frac{-Ea}{RT}\right\} \quad (1)$$

where $A$ is the pre-exponential factor, which is a constant for the specific reaction, $n_F$ is the concentration of fluorine radicals on the surface. $Ea$ is the activation energy for the chemical reaction, $R$ is the universal gas constant and $T$ is the absolute temperature of the sample surface. At the dislocation sites, stress energy which promotes the etching process exists.[9] Thus, the activation energy of the dislocation sites should be slightly smaller than that of the perfect crystal surface and the difference is expressed as $\Delta E$. Then the expression of $v_d$ is shown in Equation (2):

ACCEPTED MANUSCRIPT

$$v_{\mathrm{d}} = n_{\mathrm{F}} A exp \left\{ \frac{-(Ea - \Delta E)}{RT} \right\} \quad (2)$$

Then, the pitting speed, which is also the relative etching rate between $v_d$ and $v_p$ can be expressed in Equation (3):

$$v_{\mathrm{pits}} = v_{\mathrm{d}} - v_{\mathrm{p}} = n_{\mathrm{F}} A exp \left\{ \frac{-Ea}{RT} \right\} \left\{ exp \left\{ \frac{\Delta E}{RT} \right\} - 1 \right\} \quad (3)$$

As the dislocations existing in SiC are mainly linear dislocations, $\Delta E\ (RT)^{-1}$ should be a small value.[34] Thus, Equation (3) can be written into this formula:

$$v_{\mathrm{pits}} = n_{\mathrm{F}} A exp \left\{ \frac{-Ea}{RT} \right\} \left\{ exp \left\{ \frac{\Delta E}{RT} \right\} - 1 \right\} \cong n_{\mathrm{F}} A exp \left\{ \frac{-Ea}{RT} \right\} \frac{\Delta E}{RT} \quad (4)$$

In Equation (4), $n_F$, $A$ and $\Delta E$ are all considered as constants in the dry etching process and they will not change with temperature, thus, only the rest part of the equation needs to be considered. Here, $V$ was used as the temperature-dependent part of Equation (4).

$$V = \frac{v_{\mathrm{pits}}}{n_{\mathrm{F}} A \Delta E} = \exp\left(\frac{-Ea}{RT}\right) \frac{1}{RT} \quad (5)$$

Using the activation energy calculated by Sano et al.[35], the $V$ can be plotted as Figure 3c. It has been demonstrated from the plot that in the temperature range of 300-1000 K, the pitting speed for dislocation sites will increase greatly with the temperature. At a low temperature around 300 K, as shown in Figure 3d, the difference between $v_d$ and $v_p$ are not significant, thus, $v_{pits}$ is very small. Both perfect crystalline surface and dislocation sites were etched almost uniformly, thus no etching pits stands for dislocations could be formed. However, at a high temperature around 1000 K, $v_{pits}$ can be more than 1000 times

ACCEPTED MANUSCRIPT

higher than that at low temperature, thus, dislocations could be reveled efficiently as demonstrated in Figure 3e.

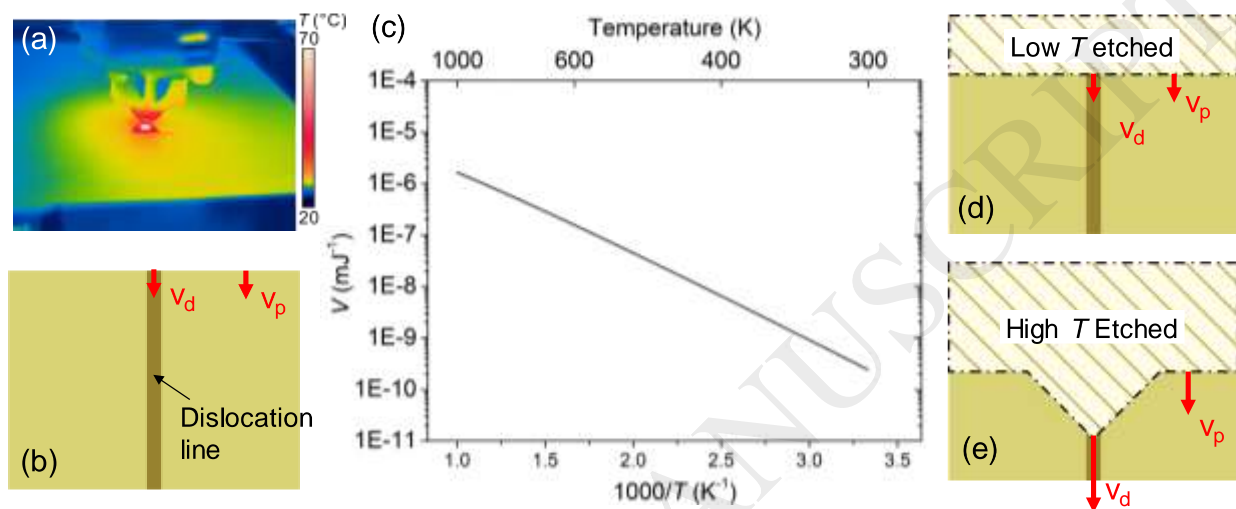


Figure 3. a) Thermal image of the substrate during CCP etching. b, d, e) Schematic of 4H-SiC with a threading dislocation line (b) before etching, (d) after low temperature etching and (e) high temperature etching. c) The Arrhenius style plot of V-Temperature.

ACCEPTED MANUSCRIPT

ACCEPTED MANUSCRIPT

### 3.4 ICP Etching

According to the dislocation revelation mechanisms discussed above, dry etching is not the sufficient condition to reveal dislocation, a high etching temperature is indispensable. Atmospheric pressure ICP has been generally admitted to possess both higher temperature (5000-7000 K) and higher radical density ($10^{13}$-$10^{17}$ $cm^{-3}$).[36] Thus, ICP is supposed to be an ideal plasma source for dislocation revelation applications. Figure 4a shows the schematic of the ICP setup used in this study. The optical photo of the plasma is shown in Figure 4b. The radical compositions in the plasma without and with $CF_4$ addition were confirmed by measurement of OES spectra, and the results are shown in Figure 4c. After $CF_4$ was added into the ignition gas, strong peaks corresponding to CFx and $C_2$ radicals were detected, and the intensity of argon decreased a lot.[31, 37] The emissions from fluorine radicals couldn't be detected which was considered owing to overlap with the strong peaks corresponding to argon. However, the existence of strong $CF_x$ radicals and $C_2$ radicals proves the dissociation of $CF_4$ and the generation of fluorine radicals which have a very strong oxidation potential.[38]

Thermal image (Figure 4e) of the SiC sample during ICP etching shows the average surface temperature of the sample was 350°C and the maximum temperature was 458.7°C. Therefore, the pitting speed to reveal dislocations could be more than 1000 times higher than that operating at room temperature according Figure 3e. The OES spectra and thermal image suggest that the $CF_4$-based ICP etching should be applicable for dislocation revelation of SiC wafers.

ACCEPTED MANUSCRIPT

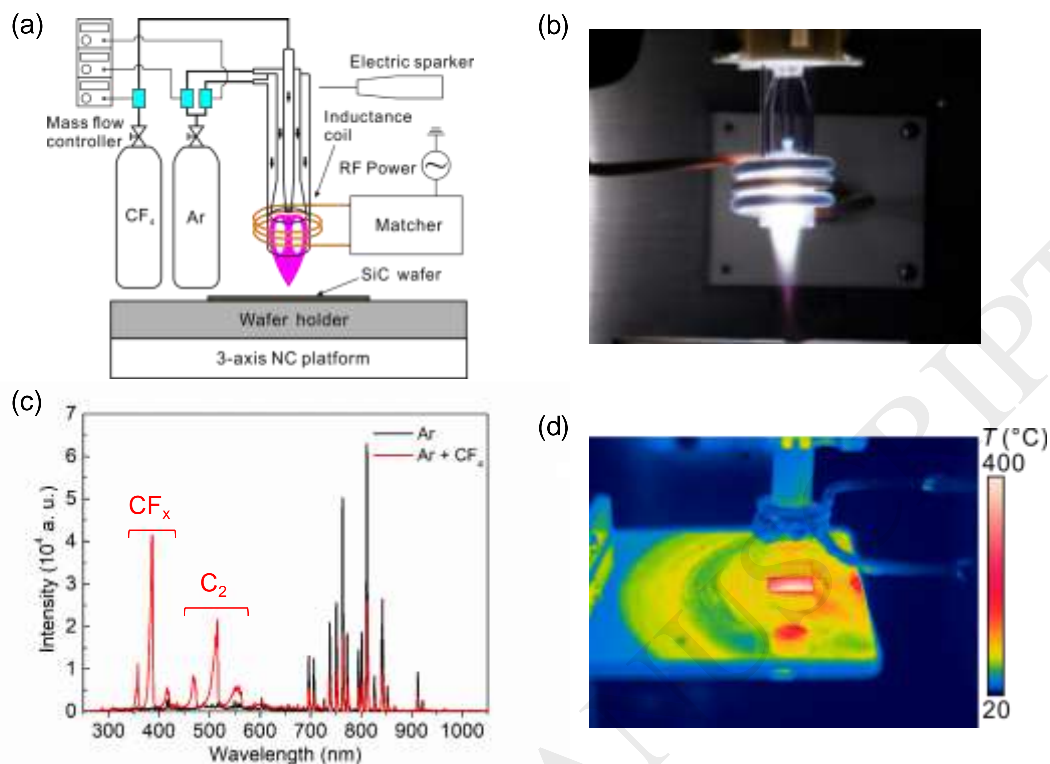


Figure 4. a) Schematic diagram of experimental setup for ICP plasma etching. b) optical photo of the ICP jet. c) OES spectra of the ICP jet without and with $CF_4$ addition. d) thermal image of the substrate during ICP etching.

ICP etching was then carried out on the Si-face of a 4H-SiC wafer, and the results are shown in Figure 5. Figure 5a shows the SEM image of the etched surface, many hexagonal etching pits were formed as forecasted. Those hexagonal etching pits can be mainly divided into two groups. The larger hexagonal etching pits stand for micropipes and TSDs, and the smaller etching pits stand for TEDs. A close up view of a micropipe-originated etching pit is shown in Figure 5b. It is a bottomless hexagonal pit as most

ACCEPTED MANUSCRIPT

micropipes are deep and threading through the whole wafer.[39] Figure 5c shows an etching pit originated from a TSD. It is much bigger than etching pits originated from TEDs as shown in Figure 5d. The size difference of etching pits is originating from the difference of pitting speeds for each type of dislocations, which is further determined by the difference of strain energy at the dislocation sites. The strain energy of dislocations is proportional to the square of its burger vector.[9] No seashell-shape etching pits corresponding to BPDs has been observed on this sample. This was considered owing to the dislocation conversion effect.[40] Figure 5e shows the surface morphology of the pit-free area of the wafer. Without pronounced etching pits standing for dislocations, this surface is supposed to be the perfect crystalline surface. However, it is still covered by visually uniform small etching pits. It is suggested to be the result of preferential etching caused by thermal noise. According to Arrhenius equation, as the average temperature of this sample is very high during ICP etching, a small random heat fluctuation will cause huge difference in etching rate.[32] Thus, countless uniform small etching pits was formed on the surface. These results prove that the proposal to reveal dislocations in SiC using ICP etching is effective.

ACCEPTED MANUSCRIPT

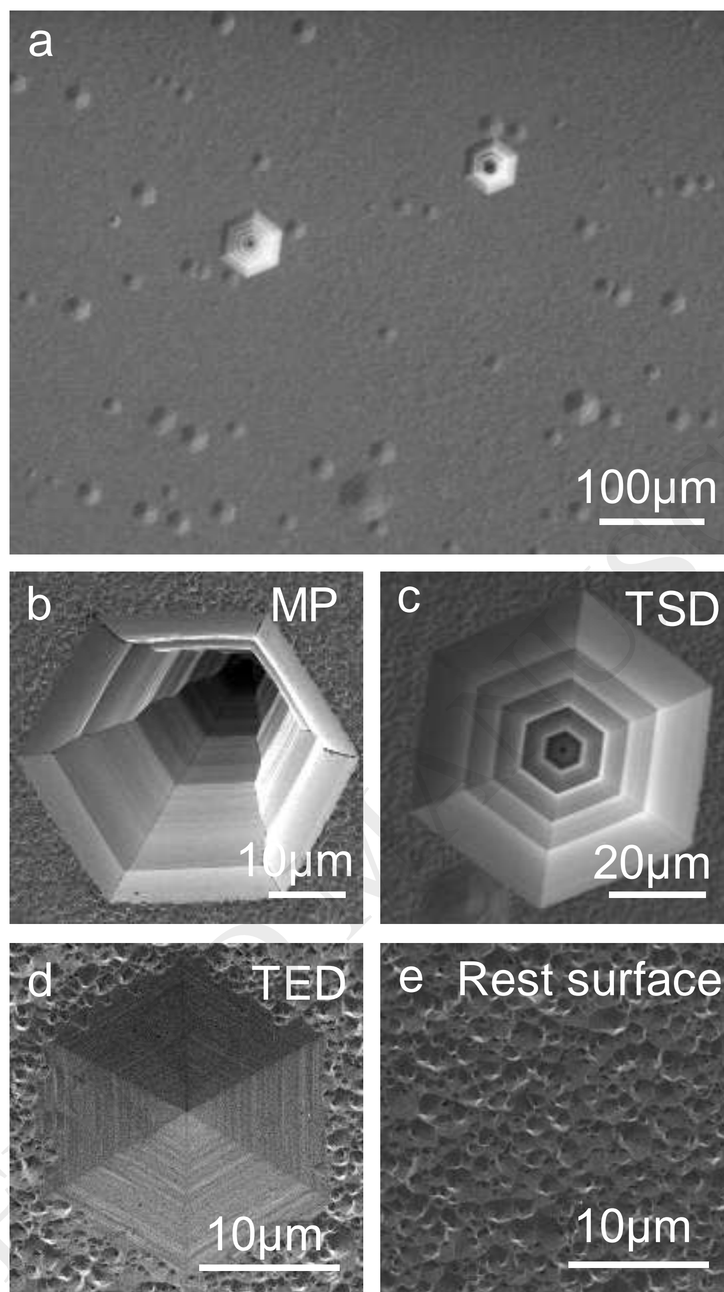


Figure 5. a) SEM image of the ICP etched surface of SiC and the close-up SEM image of b) MP; c) TSD; d) TED and e) the rest surface.

ACCEPTED MANUSCRIPT

### 3.5. Comparative study between molten KOH etching and ICP etching

To compare the dislocation revelation ability of conventional molten KOH etching method and ICP etching method for 4H-SiC with different doping concentrations, comparative experiments were carried out. To insure the dislocation density for the high doping sample and low doping sample are similar, a SiC wafer contains both low doping area and high doping area was used (Figure 6a). This wafer was cut into two SiC sheets, both in approximate 10 mm×20 mm size. And both sheets contain low doping area and high doping area with almost the same proportion as marked. One SiC sheet was treated with conventional method (marked no. 1) and the other with ICP etching method (marked no. 2) and then the results are being discussed.

ACCEPTED MANUSCRIPT

ACCEPTED MANUSCRIPT

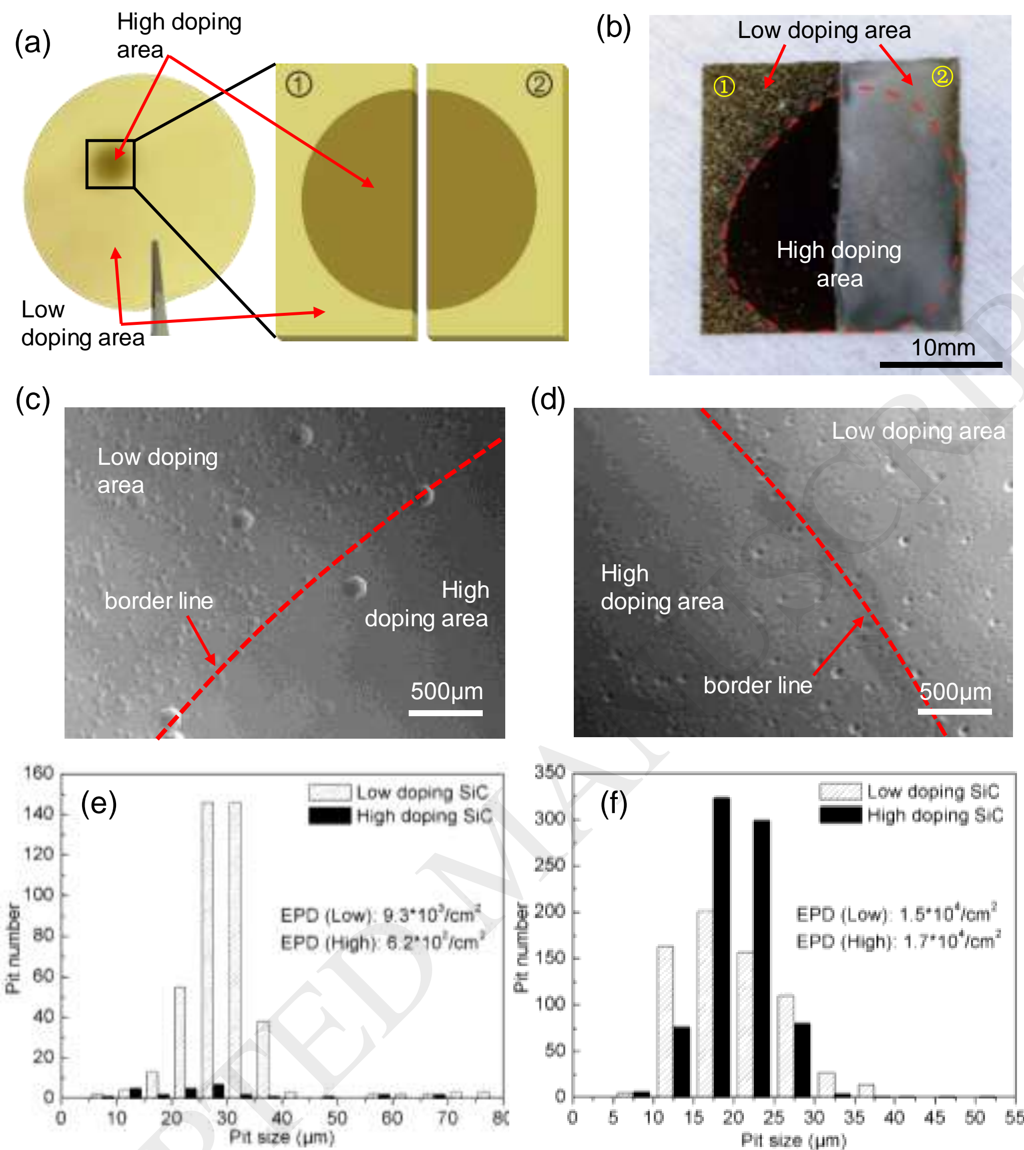


Figure 6. a) Optical photo of the SiC wafer used (left) and the schematic of the two samples cut off from that wafer (right). b) Optical photo of the samples after conventional molten KOH etching and ICP etching respectively. c, d) SEM images for the boundary area between low doping area and high doping area of SiC etched by (c) conventional method and (d) plasma etching method. e, f) Size distribution of etching pits of the low and high doping areas for SiC samples processed by (e) molten KOH etching and (f) plasma etching.

ACCEPTED MANUSCRIPT

As shown in Figure 6b, the left part is the sample treated with conventional molten KOH etching method. The surface morphologies are obviously different between the low doping area and high doping area, which has also been proved by the SEM observation covering the boundary area as shown in Figure 5c. The low doping area is covered by uniform distributed etching pits, with size separated into two groups. This implies that dislocations are well detected in this area. However, for the high doping area, only few etching pits can be recognized. Most area remains a specular surface, suggesting isotropic etching was dominate and dislocations have not been revealed efficiently. For the right part in Figure 6b, which is the sample treated with ICP etching method, the whole SiC sheet is visually uniform. Both high and low doping areas are covered with etching pits as demonstrated by the SEM image shown in Figure 6d. With the border being marked using a mark line, no significant difference can be found across the border.

To further evaluate the dislocation revelation results, EPD has been employed to show the density of dislocations exposed at the etched surfaces. Figure 6e shows the size distribution of the etching pits on a SiC sample etched by molten KOH. The number of etching pits with different sizes were quite different for the lightly doped and highly doped areas. The number of etching pits counted for low doping area was 419, while only 28 etching pits were observed for the high doping area. The EPD for low doping area is $9.3\times10^{3}$ $cm^{-2}$, it is lightly lower than the EPD measured by ICP etching as well as the typical dislocation density of 4H-SiC substrate, which is $10^{4}$ $cm^{-2}$. It means that even for the relatively lightly doped area, the measured EPD using molten KOH etching method is still questionable. As for the EPD measured on the highly doped area, it is only $6.2\times10^{2}$ $cm^{-2}$, which is far below the actual value. The size distribution of etching pits on SiC after

ACCEPTED MANUSCRIPT

ICP etching has been shown in Figure 6f. The number of etching pits for the two areas on this sample was very close. 680 etching pits were found on the low doping area and 789 etching pits were found on the high doping area. EPDs for the low doping area and high doping area are $1.5\times10^4$ $cm^{-2}$ and $1.7\times10^4$ $cm^{-2}$ respectively, which are very close to the specific value. These results demonstrate that ICP etching is an effective and accurate approach for dislocation revelation for both low doping and high doping SiC.

## 4. Conclusions

In summary, we have demonstrated in this work that indiscriminate and accurate dislocation revelation of single crystal SiC can be realized using ICP etching. Conventional molten KOH etching method failed to reveal the dislocations in the highly doped wafer area owing to the occurring of isotropic electrochemical etching phenomenon. To avert the electrochemical etching problem, plasma dry etching was utilized. On the basis of CCP etching results and plasma etching kinetics analysis, it has been proved that dislocation revelation in plasma dry etching is highly related to the process temperature. While the low temperature CCP etching process also failed to realize the anisotropic etching of dislocation sites, the developed ICP etching method demonstrated the ability to effectively reveal the dislocations in SiC wafers regardless of the doping concentration. This will provide designers with a wealth of information for higher quality single crystal SiC wafers in an early stage of the product process in semiconductor manufacturing.

ACCEPTED MANUSCRIPT

**Acknowledgements**

This work was financially supported by the Start-up Funding from the Southern University of Science and Technology (33/Y01336106), the research fund for Basic Research (Free Exploration) and the research fund for International Cooperation from the Science and Technology Innovation Committee of Shenzhen Municipality (201803023000850/201809283000307). This work was also supported by the Pico Center at SUSTech that receives support from Presidential fund and Development and Reform Commission of Shenzhen Municipality.

ACCEPTED MANUSCRIPT

ACCEPTED MANUSCRIPT

## REFERENCES

1. Bhatnagar, M.; Baliga, B. J., Comparison of 6H-SiC, 3C-SiC, and Si for power devices. *IEEE Trans. Electron Devices* 1993, *40* (3), 645-655.

2. Nakamura, D.; Gunjishima, I.; Yamaguchi, S.; Ito, T.; Okamoto, A.; Kondo, H.; Onda, S.; Takatori, K., Ultrahigh-quality silicon carbide single crystals. *Nature* 2004, *430* (7003), 1009-1012.

3. Frank, F., Capillary equilibria of dislocated crystals. *Acta Crystallographica* 1951, *4* (6), 497-501.

4. Eddy, C.; Gaskill, D., Silicon carbide as a platform for power electronics. *Science* 2009, *324* (5933), 1398-1400.

5. Berechman, R.; Skowronski, M.; Soloviev, S.; Sandvik, P., Electrical characterization of 4H–SiC avalanche photodiodes containing threading edge and screw dislocations. *J. Appl. Phys.* 2010, *107* (11), 114504.

6. Maximenko, S.; Freitas Jr, J.; Myers-Ward, R.; Lew, K.-K.; VanMil, B.; Eddy Jr, C.; Gaskill, D.; Muzykov, P.; Sudarshan, T., Effect of threading screw and edge dislocations on transport properties of 4H–SiC homoepitaxial layers. *J. Appl. Phys.* 2010, *108* (1), 013708.

7. Katsuno, M.; Ohtani, N.; Takahashi, J.; Yashiro, H.; Kanaya, M., Mechanism of molten KOH etching of SiC single crystals: comparative study with thermal oxidation. *Jpn. J. Appl. Phys.* 1999, *38* (8R), 4661.

8. Yakimova, R.; Hylen, A.; Tuominen, M.; Syvajarvi, M.; Janzen, E., Preferential etching of SiC crystals. *Diamond Relat. Mater.* 1997, *6* (10), 1456-1458.

9. Sakwe, S.; Müller, R.; Wellmann, P., Optimization of KOH etching parameters for

ACCEPTED MANUSCRIPT

quantitative defect recognition in n-and p-type doped SiC. *J. Cryst. Growth* 2006, *289* (2), 520-526.

10. Zhuang, D.; Edgar, J., Wet etching of GaN, AlN, and SiC: a review. *Mater. Sci. Eng., R* 2005, *48* (1), 1-46.

11. Yao, Y.-Z.; Ishikawa, Y.; Sugawara, Y.; Saitoh, H.; Danno, K.; Suzuki, H.; Kawai, Y.; Shibata, N., Molten KOH etching with Na2O2 additive for dislocation revelation in 4H-SiC epilayers and substrates. *Jpn. J. Appl. Phys.* 2011, *50* (7R), 075502.

12. Gao, Y.; Zhang, Z.; Bondokov, R.; Soloviev, S.; Sudarshan, T., The Effect of Doping Concentration and Conductivity Type on Preferential Etching of 4H-SiC by Molten KOH. *MRS Online Proceedings Library Archive* 2004, *815*.

13. Wu, P., Etching study of dislocations in heavily nitrogen doped SiC crystals. *J. Cryst. Growth* 2010, *312* (8), 1193-1198.

14. Liu, N.; Yi, R.; Deng, H., Study of initiation and development of local oxidation phenomena during anodizing of SiC. *Electrochem. Commun.* 2018, *89*, 27-31.

15. Jia, G.; Li, B.; Zhang, J., Influence of SiC surface defects on materials removal in atmospheric pressure plasma polishing. *Comput. Mater. Sci.* 2018, *146*, 26-35.

16. Kallinger, B.; Polster, S.; Berwian, P.; Friedrich, J.; Müller, G.; Danilewsky, A.; Wehrhahn, A.; Weber, A.-D., Threading dislocations in n-and p-type 4H–SiC material analyzed by etching and synchrotron X-ray topography. *J. Cryst. Growth* 2011, *314* (1), 21-29.

17. Song, H.; Sudarshan, T. S., Basal plane dislocation conversion near the epilayer/substrate interface in epitaxial growth of 4° off-axis 4H–SiC. *J. Cryst. Growth* 2013, *371*, 94-101.

ACCEPTED MANUSCRIPT

18. Zhang, Z.; Gao, Y.; Sudarshan, T., Delineating structural defects in highly doped n-type 4H-SiC substrates using a combination of thermal diffusion and molten KOH etching. *Electrochem. Solid-State Lett.* 2004, *7* (11), G264-G265.

19. Shor, J.; Zhang, X.; Osgood, R., Laser‐Assisted Photoelectrochemical Etching of n‐type Beta‐SiC. *J. Electrochem. Soc.* 1992, *139* (4), 1213-1216.

20. Shor, J.; Osgood, R.; Kurtz, A., Photoelectrochemical conductivity selective etch stops for SiC. *Appl. Phys. Lett.* 1992, *60* (8), 1001-1003.

21. Henisch, H. K., *Rectifying semi-conductor contacts*. Clarendon Press: 1957.

22. Kittel, C.; McEuen, P.; McEuen, P., *Introduction to solid state physics*. Wiley New York: 1996; Vol. 8.

23. Haus, J. W., *Fundamentals and applications of nanophotonics*. Woodhead Publishing: 2016.

24. Pankaj, S. K.; Bueno-Ferrer, C.; Misra, N.; Milosavljevi , V.; O'donnell, C.; Bourke, P.; Keener, K.; Cullen, P., Applications of cold plasma technology in food packaging. *Trends Food Sci. Technol.* 2014, *35* (1), 5-17.

25. Liang, D. C.; Blades, M., Atmospheric pressure capacitively coupled plasma atomizer for atomic absorption spectrometry. *Anal. Chem.* 1988, *60* (1), 27-31.

26. Yih, P.; Saxena, V.; Steckl, A., A review of SiC reactive ion etching in fluorinated plasmas. *Phys. Status Solidi B* 1997, *202* (1), 605-642.

27. Nisticò, R.; Magnacca, G.; Faga, M. G.; Gautier, G.; D'Angelo, D.; Ciancio, E.; Lamberti, R.; Martorana, S., Effect of atmospheric oxidative plasma treatments on polypropylenic fibers surface: Characterization and reaction mechanisms. *Appl. Surf. Sci.* 2013, *279*, 285-292.

ACCEPTED MANUSCRIPT

28. Zhu, W.-C.; Li, Q.; Zhu, X.-M.; Pu, Y.-K., Characteristics of atmospheric pressure plasma jets emerging into ambient air and helium. *J. Phys. D: Appl. Phys.* 2009, *42* (20), 202002.

29. Ren-Wu, Z.; Xian-Hui, Z.; Zi-Chao, Z.; Jun-Xiong, L.; Zhou-Bin, Y.; Dong-Ping, L.; Si-Ze, Y., Reactive oxygen species in plasma against E. coli cells survival rate. *Chin. Phys. B* 2015, *24* (8), 085201.

30. Resnik, M.; Zaplotnik, R.; Mozetic, M.; Vesel, A., Comparison of SF6 and CF4 Plasma Treatment for Surface Hydrophobization of PET Polymer. *Materials* 2018, *11* (2), 311.

31. Wang, R.; Zhang, C.; Liu, X.; Xie, Q.; Yan, P.; Shao, T., Microsecond pulse driven Ar/CF4 plasma jet for polymethylmethacrylate surface modification at atmospheric pressure. *Appl. Surf. Sci.* 2015, *328*, 509-515.

32. Laidler, K. J., The development of the Arrhenius equation. *J. Chem. Educ.* 1984, *61* (6), 494.

33. Castelli, M.; Jourdain, R.; Morantz, P.; Shore, P., Rapid optical surface figuring using reactive atom plasma. *Precis. Eng.* 2012, *36* (3), 467-476.

34. Habuka, H., Etching of Silicon Carbide Using Chlorine Trifluoride Gas. In *Physics and Technology of Silicon Carbide Devices*, InTech: 2012.

35. Sano, Y.; Watanabe, M.; Kato, T.; Yamamura, K.; Mimura, H.; Yamauchi, K. In *Temperature dependence of plasma chemical vaporization machining of silicon and silicon carbide*, Mater. Sci. Forum, Trans Tech Publ: 2009; pp 847-850.

36. Ichiki, T.; Taura, R.; Horiike, Y., Localized and ultrahigh-rate etching of silicon wafers using atmospheric-pressure microplasma jets. *J. Appl. Phys.* 2004, *95* (1), 35-

ACCEPTED MANUSCRIPT

39.

37. Jung, T.; Kim, D.; Lim, H., Molecular Emission of CF 4 Gas in Low-pressure Inductively Coupled Plasma. *Bull. Korean Chem. Soc.* 2006, *27* (3), 373-375.

38. Zimmermann, S.; Ahner, N.; Blaschta, F.; Schaller, M.; Rülke, H.; Schulz, S.; Gessner, T., Analysis of the impact of different additives during etch processes of dense and porous low-k with OES and QMS. *Microelectron. Eng.* 2010, *87* (3), 337-342.

39. Dudley, M.; Huang, X.; Huang, W.; Powell, A.; Wang, S.; Neudeck, P.; Skowronski, M., The mechanism of micropipe nucleation at inclusions in silicon carbide. *Appl. Phys. Lett.* 1999, *75* (6), 784-786.

40. Ha, S.; Mieszkowski, P.; Skowronski, M.; Rowland, L., Dislocation conversion in 4H silicon carbide epitaxy. *J. Cryst. Growth* 2002, *244* (3-4), 257-266.

ACCEPTED MANUSCRIPT